A micro-mechanical insight into the thermo-mechanical behaviour of clays

Alice Di Donna
Université Grenoble Alpes, CNRS, Grenoble INP, 3SR, Grenoble (France)
alice.di-donna@univ-grenoble-alpes.fr
ORCID: 0000-0002-4383-852X

Angela Casarella
Université Grenoble Alpes, CNRS, Grenoble INP, 3SR, Grenoble (France)
angela.casarella@chalmers.se
ORCID: 0009-0005-8825-4922

Alessandro Tarantino
Department of Civil and Environmental Engineering, University of Strathclyde (Scotland, UK)
alessandro.tarantino@strath.ac.uk
ORCID: 0000-0001-6690-748X

Abstract

The response of fine-grained soils to the combined effects of stress and temperature is a problem of growing concern in geoenvironmental engineering. Unlike most materials, fine-grained soils subjected to heating under drained conditions can exhibit either reversible expansion or irreversible contraction, depending on their loading history. This clay complex thermo-mechanical behaviour is widely reported in the literature, but its origin is still unknown. This paper explores the particle-scale origin of clay thermo-mechanical behaviour and helps to inform constitutive thermo-mechanical models. Clay particle interactions include non-contact forces, which are electrochemical in nature and prevail in face-to-face configuration and contact forces, which are mechanical forces transferred from one particle to another through a contact surface, typical of edge-to-face configuration. Non-contact forces include electrostatic Coulombic forces and van der Waals attractive forces. This paper proposes a combined numerical and analytical approach to quantify the elementary interactions between clay particles. The results are used to interpret typical stress-thermal paths, such as compression tests at different temperatures and heating-cooling cycles at constant mechanical stress. It is concluded that the electrochemical interactions governing the face-to-face particle configuration can only explain the elastic volumetric response of over-consolidated clays subjected to heating. The thermo-plastic behaviour associated with the reduction of the pre-consolidation pressure with temperature and the volumetric plastic compressive strain in response to heating in normally-consolidated clays is attributed to the edge-to-face particle configurations.

Keywords: clay thermo-mechanics, clay micromechanics, contact and non-contact inter-particle forces

1 INTRODUCTION

The effect of temperature on the mechanical behaviour of geomaterials is a problem of growing concern in geoenvironmental engineering. The response of soils to the combined effects of stress and temperature has been investigated in depth in the last decades, mainly in the context of nuclear waste geological disposal (Hueckel and Baldi 1990, Sultan et al. 2002, Romero et al. 2005), focusing on the study of high-swelling clay. The effect of temperature changes has been investigated to a lesser extent in non-active or moderately active clay, which is of interest in several applications, including shallow geothermal plants, energy geostructures (Laloui and Di Donna 2013), and heating in rapid shear deformation (Sulem et al. 2007).

Energy geostructures are ground-embedded structures such as shallow foundations, bored piles, diaphragm walls, tunnel cut-and-cover walls and tunnel linings systems that can be used as ground heat exchanger elements. The soil is used as a thermal bank where heat is deposited in summer (heat sink) and withdrawn in winter (heat source). In many countries, the development of this technology is lagging owing to the difficulty of characterising and modelling the thermo-hydro-mechanical (THM) behaviour of fine-grained soils (Di Donna et al. 2017). Most of the uncertainties regarding the geotechnical behaviour of energy geostructures are related to the volumetric behaviour of soft clay and the potential generation of over-structure settlements.

Unlike most materials that undergo a reversible expansion upon heating, fine-grained soils subjected to heating under drained conditions can exhibit either reversible expansion or irreversible contraction, depending on their loading history. This clay complex non-linear and irreversible thermo-mechanical behaviour is largely documented in the literature at the laboratory scale. Advanced continuum constitutive models have been developed and employed to reproduce such behaviour at the engineering scale (Hueckel and Baldi 1990, Modaressi and Laloui 1997, Cui et al. 2000, Graham et al. 2001). However, those models are purely phenomenological and require the calibration of large sets of parameters against time-consuming and relatively expensive experimental tests. The origin of such non-intuitive behaviour can be unveiled by exploring particle-scale interactions, which could, in turn, help build physically-informed constitutive models.

For granular materials, experimental observation at the grain scale has proven to be a valuable tool to improve our understanding of the macroscopic behaviour of coarse-grained soils. ‘In-situ’ observation of the evolution of clay fabric (at the scale of tens to hundreds of nanometers) is very challenging and beyond the capability of current XCT equipment. As a result,

mechanisms at the particle scale controlling the macro-mechanical behaviour of clay are still largely ignored. The lack of experimental evidence makes discrete modelling, including Discrete Element Method (DEM) and Coarse-Grained Molecular Dynamics (CGMD), a complementary tool to investigate particle-scale mechanisms driving clay mechanical macroscopic response. This approach is based on the mathematical determination of the forces between clay particles, which must include the contact forces between the particles and the interactions deriving from the electrochemical forces arising from the clay particle's electrical charge. In this paper, a combined numerical and analytical approach is proposed to quantify these complex interactions between clay particles. A different approach to investigate the same problem was proposed by Brochard et al. (2018), who attributed the macroscopic thermo-mechanical response of clay to water adsorption between clay unit layers at the nanometer scale. This proposition gains significance when examining clay minerals with substantial adsorbed water content, as seen in swelling clays, where tens of % of total water is absorbed in saturated swelling clay samples. However, for non-swelling and soft clays characterised by a significant amount of bulk water compared to adsorbed water, it becomes essential also to consider temperature-induced changes in the arrangement of clay particles/aggregates, affecting inter-particle/aggregate porosity. Both approaches share the concept of examining the small scale to interpret the counterintuitive thermomechanical macroscopic behaviour of clays but diverge fundamentally in their hypotheses regarding the source of such behavior—whether it stems from changes in intra-particle porosity or changes in inter-particle/aggregate porosity.

The main objective of this work is to investigate whether contact and non-contact forces acting between the clay particles can explain mathematically the thermoelastic-thermoplastic behaviour of clay. This is important to corroborate, qualitatively, the hypothesis that the interaction at the small scale governs the observed behaviour. As the analysis is limited to two particles interactions, a proper upscale approach would be needed to extend the results to a larger number of particles, but this is out of the purpose of this paper. In this sense, a side goal of this work is to develop data that could be used to define and calibrate a physically-based energy separation function to feed CGMD models. Such a modelling approach would naturally include the real physics, avoiding the heavy calibration procedure of phenomenological constitutive models currently used to reproduce the thermo-mechanical behaviour of clay.

2 MACROSCOPIC THERMO-MECHANICAL BEHAVIOUR OF CLAYS

The mechanical response of clay upon heating and cooling is not always intuitive. Early experimental results focusing on the thermally induced deformation of (saturated) fine-grained soils have been obtained, among others, by Campanella and Mitchell (1968), Baldi et al. (1988), Hueckel and Baldi (1990) and have been widely confirmed by recent literature (Del Olmo et al. 1996, Cekerevac and Laloui 2004, Abuel-Naga et al. 2009, Di Donna and Laloui 2015). The evidence shows that heating clayey soils under drained conditions can produce either a contractive or a dilative volume variation, depending on whether the soil is Normally Consolidated (NC) or Over Consolidated (OC). The variation of the thermally induced volumetric strain, ε_v [%], with applied temperature variation, ΔT [°C], characterising a variety of fine-grained soils at different Over-Consolidation Ratios (OCR) is reported in Figure 1a. The material undergoes irreversible and non-linear contraction upon heating in NC conditions (OCR=1) (thermo-plasticity), while OC soils (OCR>>1) experience a reversible volume expansion during heating (thermo-elasticity). An intermediate case is represented by slightly OC clays (OCR>1): the material shows initial dilation and subsequent contraction upon heating, followed by contraction during cooling. From these results, it is clear that the volumetric response of clayey soils to temperature cannot be explained solely in terms of thermal expansion of the solid and pore fluid phases, as is the case of granular materials. Complementary experimental results presented in Figure 1b also show that yielding along compression paths at higher temperature occurs at stresses lower than the maximum stress experienced at the reference temperature (Eriksson 1989, Tidfors and Sällfors 1989, Boudali et al. 1994, Moritz 1995, Di Donna and Laloui 2015). In other words, the clay exhibits an 'apparent' preconsolidation stress at higher temperatures lower than the actual pre-consolidation stress at the reference temperature (thermally induced softening). Additionally, Towhata et al. (1993) and Burghignoli et al. (2000) observed that the volumetric behaviour of overconsolidated clays is not always contractive, but also depends on whether they were being unloaded or reloaded prior to heating. A constitutive model able to reproduce such response was porposed by Coccia and McCartney (2016) using the concept of thermally-accelerated secondary compression, but without any consideration on the possible physical origin governing it at the microscale.

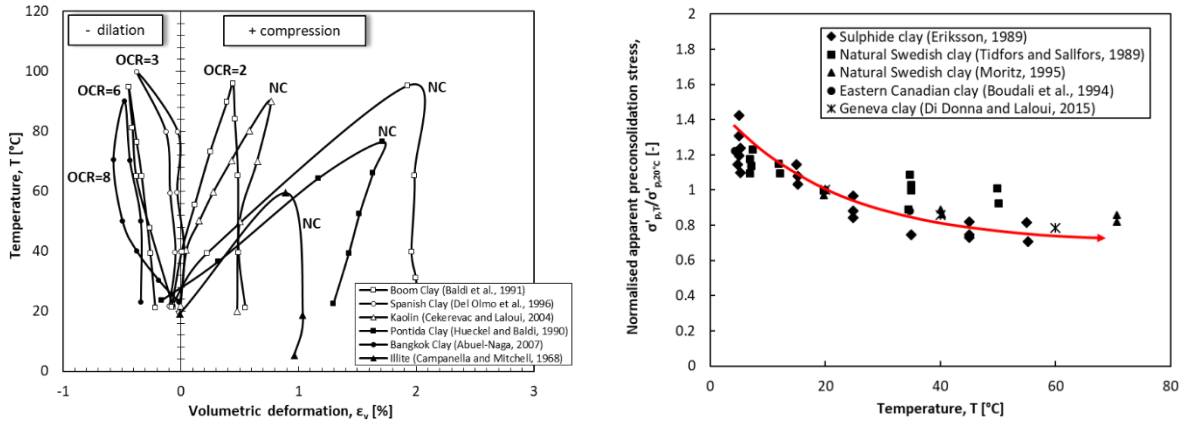

(a) (b)

Figure 1. Macroscopic observed behaviour of clays subjected to thermal loading: (a) volumetric response under constant mechanical stress and (b) effect of temperature on the preconsolidation pressure.

2.1 Selected clay material

As depicted in Figure 1, similar results have been obtained for various clayey materials containing variable fractions of illite, kaolinite, chlorite and smectite. Among them, the work presented in this paper focuses on mono-mineral kaolinite clay. It should be noted that the results on kaolinite cannot be directly extended to more complex natural clayey materials, which generally are a mixture of particles of different sizes and mineralogy; however, these represent a first step into the understanding of the fundamental physical mechanisms. Scanning Electron Microscopy (SEM) images of kaolin clay provided by Frost et al. (2004) have revealed that clay stacks often result in hexagonal plate-like shapes with a thickness-to-length ratio of about 1/10 (Figure 2).

Thanks to the peculiar 'non-swelling' nature of this material, it is possible to assume that its unit layer distance is constant and is not affected by changes in the pore-fluid properties (Pedrotti and Tarantino 2017) or temperature (Mitchell and Soga 2005). Therefore, the particle itself is considered hereafter as the elementary unit. Previous studies revealed that kaolin clay particles are characterised by a negatively charged surface and positively charged edges when exposed to an acidic pore fluid (pH < 5), while they are negatively charged all around when exposed to a more alkaline environment (pH>5-6). In the first case, an open card-house structure prevails with particles arranged in edge-to-face configuration (Figure 2a), while a close face-to-face configuration is globally observed in the second case (Figure 2b).

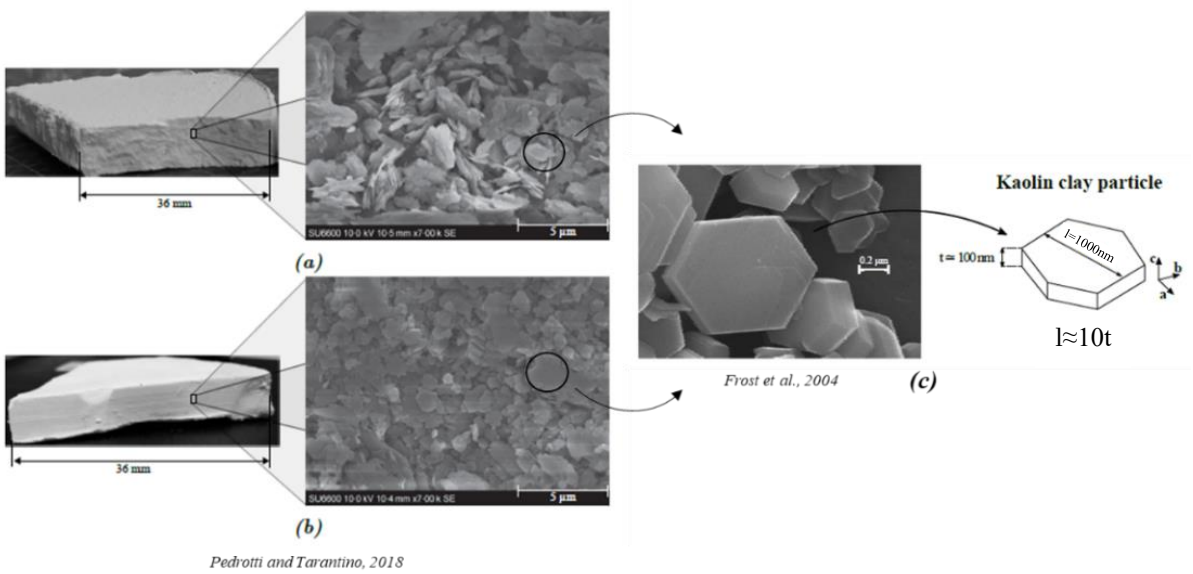

Figure 2. Kaolin clay microstructure: (a) card-house configuration obtained for pH=4 conditions; (b) closed configuration obtained for pH=9 conditions; (c) shape and dimensions of a kaolin clay particle.

3 INTER-PARTICLE INTERACTIONS

Inter-particle forces can be divided into two different categories according to Sridharan and Rao (1973): (a) non-contact forces, which are electrochemical in nature and prevail in face-to-face configuration and (b) contact forces, which are mechanical forces transferred from one particle to another through a contact surface, typical of edge-to-face configuration. According to Pedrotti and Tarantino (2018), non-contact forces are responsible for reversible elastic mechanisms, while contact forces can be associated with either reversible or non-reversible mechanisms, depending on the magnitude of the applied load.

Non-contact electrochemical forces can be described according to the DLVO theory (Derjaguin and Landau 1941, Verwey and Overbeek 1948), which assumes that the interaction between two charged particles in an electrolyte solution depends on the balance of electrostatic Coulombic forces and van der Waals attractive forces acting between the particles.

While commonly used to interpret experimental findings, such as those by Mitchell and Soga (2005), Gupta and Miller (2010), Pedrotti and Tarantino (2018), the electric double layer (EDL) description within the DLVO theory relies on assumptions like low salt concentration, homogeneous surface charge, and point-like ion distribution, which are often deemed unrealistic (Güven 1992, Masliyah and Bhattacharjee 2006). Critics argue that the DLVO theory oversimplifies particle interactions, especially at distances less than 1 nm (Carrier 2014,

Ebrahimi et al. 2016). Nonetheless, inaccuracies within the 1 nm range are considered inconsequential for describing the meso-scale clay behaviour object of this study.

Coulombic forces result from the interaction between the Electric Double Layers (EDLs) of the two charged particles. The correspondent electrostatic potential tends to decay exponentially with the distance from the charged particle surface. At particle distances from 10 nm down to interatomic spacing (about 0.2 nm), weak attractive van der Waals forces also originate from the correlations in the fluctuating polarisations of nearby particles (Israelachvili 2019).

Within the DLVO framework, the electrostatic energy, U_{EDL}, can be computed from the electrical potential field, $\phi(x,y,z)$ [V], in turn, derived from the Poisson-Boltzmann equation:

$$\nabla^2\phi(x,y,z) = \frac{2n_0 ve}{\epsilon} sinh\left(\frac{ve\phi}{kT}\right) \quad [1]$$

where n_0 [ion/m^3] is the reference ions concentration taken at a considerable distance from the particle surface (here assumed equal to 1.2044E22 m^{-3}), ν [-] is the valence (here assumed equal to 1), e [C] is the charge of the electron (e=1.602E−19 C), k [J K^{-1}] is the Boltzmann constant (k=1.38E−23 J K^{-1}), T [K] is the absolute temperature and ϵ[C^{2}J^{-1}m^{-1}] is the dielectric permittivity. This latter is equal to $\epsilon_0 \cdot \epsilon_r$, with ϵ_0 the dielectric permittivity in vacuum [ϵ_0=8.8542E−12 C^{2}J^{-1}m^{-1}], ϵ_r is the relative dielectric permittivity. Eq. [1] is non-linear and must be solved numerically.

In this equation, the temperature intervenes both directly in the denominator of the hyperbolic sinus and indirectly because the dielectric permittivity of fluids is temperature-dependent. In particular, the dielectric permittivity of water decreases with increasing temperature and, in this study, it is assumed to evolve according to the empirical formulation proposed by Malmberg and Maryott (1956):

$$\epsilon_r = 87.74 - 0.4008\mathrm{T} + 9.398 \cdot 10^{-4} \cdot T^2 - 1.41 \cdot 10^{-6} \cdot T^3 \quad [2]$$

Once the electrical potential field is obtained from the numerical solution of Eq. [1], one can compute the variation of the Grand Potential, $\Omega - \Omega_0$, according to the recent work carried out by Gupta et al. (2020). Following this approach, the electrostatic free energy for planar surfaces at constant particle surface charge, U_{EDL}, can be written as:

$$U_{EDL} = \Omega - \Omega_0 = \frac{1}{A}\int_A \sigma\phi \mathrm{dA} - \int_V \frac{\epsilon}{2}|\nabla\phi|^2 + 2kTn_0\left(cosh\left(\frac{ve\phi}{kT}\right) - 1\right)dV \quad [3]$$

where A [m^2] is the particle surface area, σ [Cm^{-2}] is the charge density on the particle surface, V [m^3] is the system volume, and Ω_0 [J] is the Grand Potential of the large reservoir of electrolyte in which the charged surfaces are immersed.

Van der Waals (vdW) forces are attractive intermolecular forces, weaker than Coulombic interactions, originating from the correlated motion of electrons in adjacent colloidal particles (Mitchell and Soga 2005). The vdW interaction energy between the two squared particles having side l, in an x, y, z space can be computed as (Casarella et al. 2024b):

$$U_{vdW} = -\frac{A_H}{\pi^2}\int_0^l dm \int_{-m}^{l-m} dy \int_0^l dn \int_{-n}^{l-n} \frac{1}{(x^2+y^2+z^2)^3} dx \qquad [4]$$

where A_H [J] is the Hamaker constant, and r [m] is the distance between the particles. It is noted that the vdW energy is inversely proportionally to the cube of the distance r between two particles for the case where particles are parallel and aligned ($U_{vdW} \propto \sim \frac{1}{r^3}$). In the work presented here, the Hamaker constant was determined as the average value among those measured for alumina face, silica face and edges by Gupta and Miller (2010). Moreover, this constant was assumed to be temperature-independent, as suggested by Israelachvili (2019). Under this assumption, no significant variation of U_{vdW} is recorded upon thermal loading (Parsegian and Ninham 1970). This attractive pair interaction energy can be computed for any relative orientation between two squared plate-like particles.

The electrostatic interaction forces can be computed by partial differentiation of the electrostatic free energy, U_{EDL} (Eq. [3]), and the vdW interaction energy, U_{vdW} (Eq. [4]), respectively with respect to the six degrees of freedom characterising the relative position of the two platy particles.

3.1 Face-to-face configuration

The electrostatic interaction forces, X_{EDL}, and vdW forces, X_{vdW}, are defined as the derivative of the electrostatic free energy, U_{EDL} (Eq. [3]), and the vdW interaction energy, U_{vdW} (Eq. [4]), respectively with respect to the inter-particle distance, h (Figure 3). Numerically, the interaction forces were derived by applying a perturbation dx perpendicular to the particle's axis on one particle with respect to the other and calculating the force via the incremental ratio (Figure 3).

It results in:

$$X_{Edl} = \frac{\partial U_{Edl}}{dx}; \quad X_{vdW} = \frac{\partial U_{vdW}}{dx} \qquad [5]$$

In this way, the evolution of the non-contact forces (X_{EDL}+X_{vdW}) as a function of the inter-particle distance, h, can be evaluated at different temperatures.

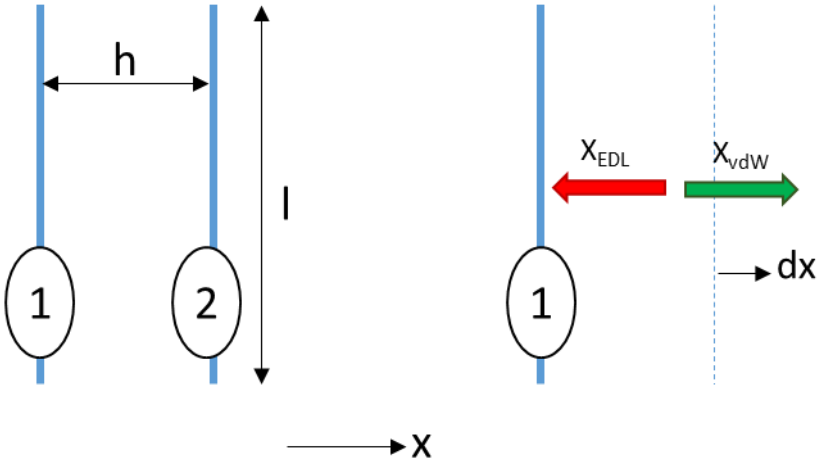

Figure 3. Non-contact forces in a system of two charged particles in face-to-face configuration.

3.2 Edge-to-face configuration

When dealing with edge-to-face configuration, contact forces also come into play. Let us consider two electrically charged particles in equilibrium in edge-to-face contact, under an applied external force, F, having a normal, F_n, and a tangential, F_t, component with respect to the particle 1 axis, as depicted in Figure 4. Besides the external force, particle 1 will also be subjected to the reaction forces applied by particle 2, which include the non-contact electrostatic interaction force and moment (due to the interacting EDLs) and the contact force. For the sake of simplicity, the vdW attraction is considered part of the contact force, which also includes the Born repulsion. The EDLs interaction force can be decomposed into a moment calculated with respect to the contact point, M_{EDL}, a normal component, N_{EDL}, and a tangential component, T_{EDL}. Similarly, the contact force, P_{con}, can be decomposed into a normal, N_{con}, and a tangential, T_{con}, component (Figure 4). For the particle equilibrium, one can write:

$$F = \frac{M_{Edl}}{d \cos \alpha} \qquad [6]$$

$$N_{con} = F_n - N_{Edl} = F\cos\alpha - N_{Edl} \quad [7]$$

$$T_{con} = F_t + T_{Edl} = F\sin\alpha + T_{Edl} \quad [8]$$

where M_{EDL}, N_{EDL} and T_{EDL} must be computed by partial differentiation of the electrostatic free energy obtained numerically, U_{EDL} (Eq. [3]), with a similar procedure to the one presented for the face-to-face configuration.

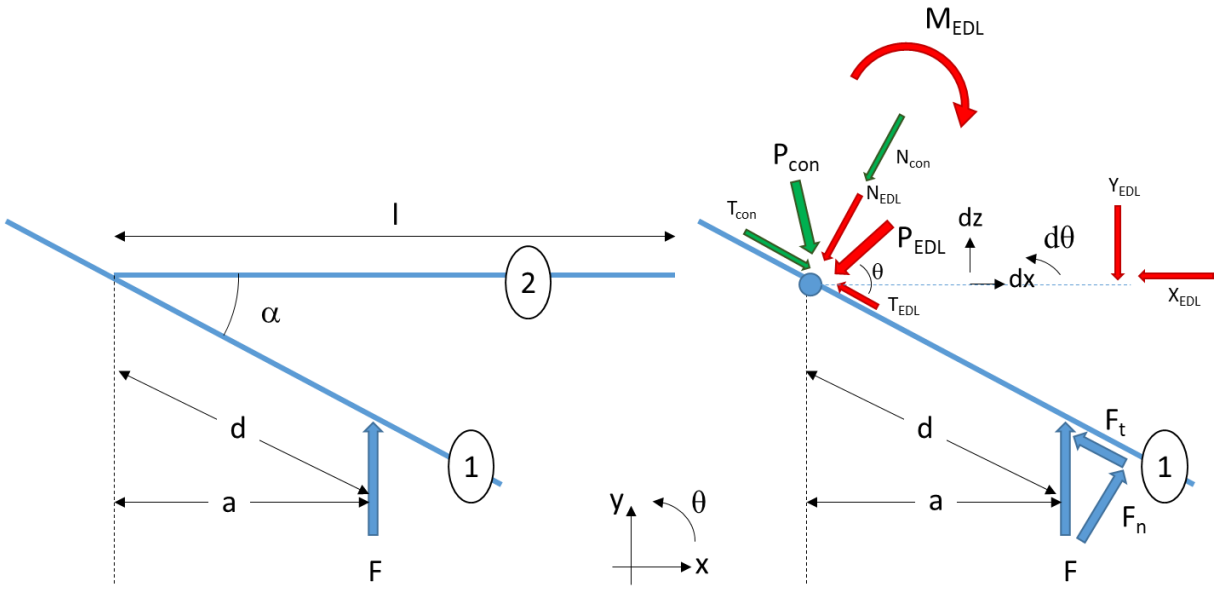

Figure 4. Balance between the applied external force, F, the Coulombic interaction, P_{EDL} and M_{EDL}, and the contact force P_{con}, in a system of two charged particles in edge-to-face configuration.

By applying a vertical, dz, a horizontal, dx, and an angular, dθ, perturbation to one particle with respect to the other, it is possible to compute:

$$M_{Edl} = \frac{\partial U_{Edl}}{d\theta} \quad [9]$$

$$N_{Edl} = \frac{\partial U_{Edl}}{dx}\sin\alpha + \frac{\partial U_{Edl}}{dy}\cos\alpha \quad [10]$$

$$T_{Edl} = \frac{\partial U_{Edl}}{dx}\cos\alpha - \frac{\partial U_{Edl}}{dy}\sin\alpha \quad [11]$$

For a given geometric configuration (i.e., the angle α between the particles) and lever arm d, the applied external force, F, and the normal, N_{con}, and tangential, T_{con}, components of the contact force (Figure 4) can be derived via Eqs. [6] to [8] once the EDL forces are derived via

Eqs. [9] to [11]. The results presented hereafter are based on d=50 nm, but a sensitivity study showed that the results do not change qualitatively for other lever arm values.

The mobilised friction angle, φ_{mob}, at the contact point between two particles in edge-to-face configuration can be derived as follows:

$$\varphi_{mob} = \text{atan}\left(\frac{T_{con}}{N_{con}}\right) \quad [12]$$

This can provide interesting information on the stability of the system made of two particles under different combinations of mechanical and thermal loading.

4 NUMERICAL MODELLING

As mentioned above, Eq. [1] can only be solved numerically, and this is needed for the calculation of U_{EDL} (Eq. [3]). To this end, an approach based on the Finite Element Method (FEM) has been employed in this work. Four different models were built in the FEM platform COMSOL Multiphysics ©, each including two interacting particles in different configurations:

- face-to-face configuration and uniform negative charge (Figure 5a);
- face-to-face configuration with edges positively charged and surface negatively charged (Figure 5b);
- edge-to-face configuration and uniform negative charge (Figure 6a);
- edge-to-face configuration with edges positively charged and surface negatively charged (Figure 6a).

Particles were modelled as squared plates with infinitesimal thickness of finite size (side l=1μm) immersed into a boxlike discretised domain where the PB equation was solved (Eq. [1]). As boundary conditions, ϕ=0 was imposed on all outer surface boundaries of the box domain, and $\mathbf{n}\cdot\nabla\phi=-\sigma/\epsilon$ was imposed on the surface of the particles, **n** being the outer normal vector. This corresponds to a constant surface charge assumption. In the cases of two parallel particles, the symmetry of the problem allowed modelling only half of the domain (Figure 5).

The negative surface charge density was assumed equal to -2 mC/m^2 in all cases, while the positive charge imposed on the edges was assumed equal to +0.25 mC/m^2, that is 1/8 of the surface charge in absolute value (Casarella 2022). The electrostatic potential, ϕ, around the charged plates in the electrolyte solution practically vanishes at a distance of 300 nm outward from the charged plate surfaces. The size of the boxlike domain was adapted accordingly for

each simulation to ensure no boundary effects. For the cases where particles were modelled with positively charged edges, the potential decreases faster as the edges' charge is lower than the one of the central surface (see later), allowing for a smaller domain.

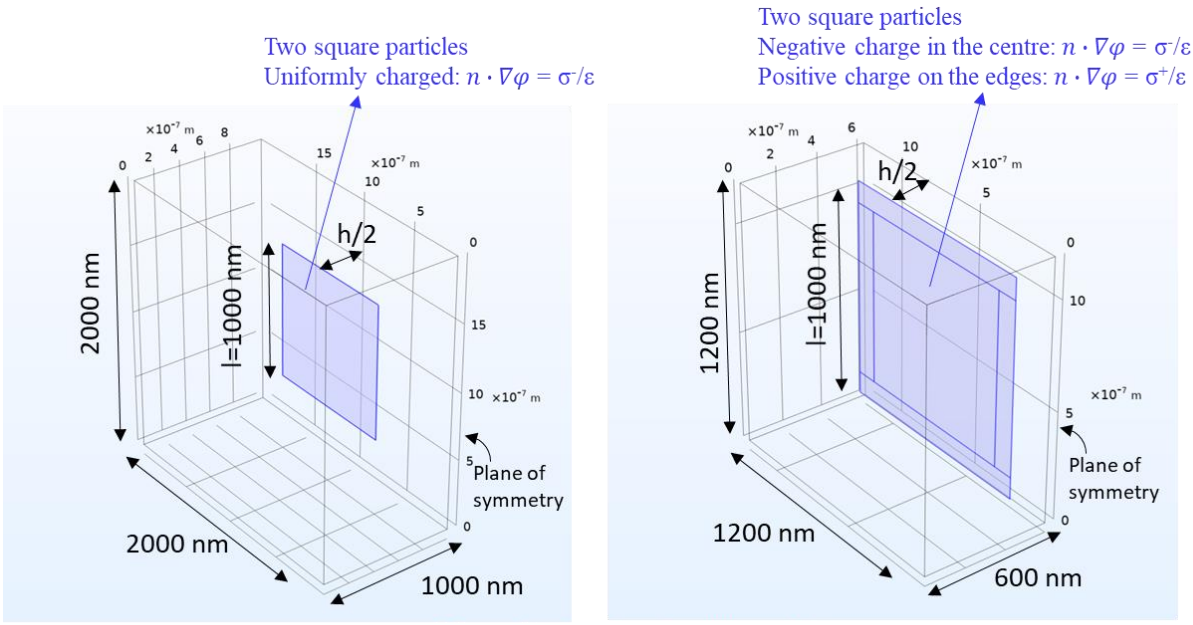

(a) (b)

Figure 5. Finite element models used to solve the Poisson-Boltzmann equation between two interacting particles in face-to-face configuration (half domain taking advantage of the symmetry): (a) with uniform negative charge; (b) with positively charged edges and negatively charged surface.

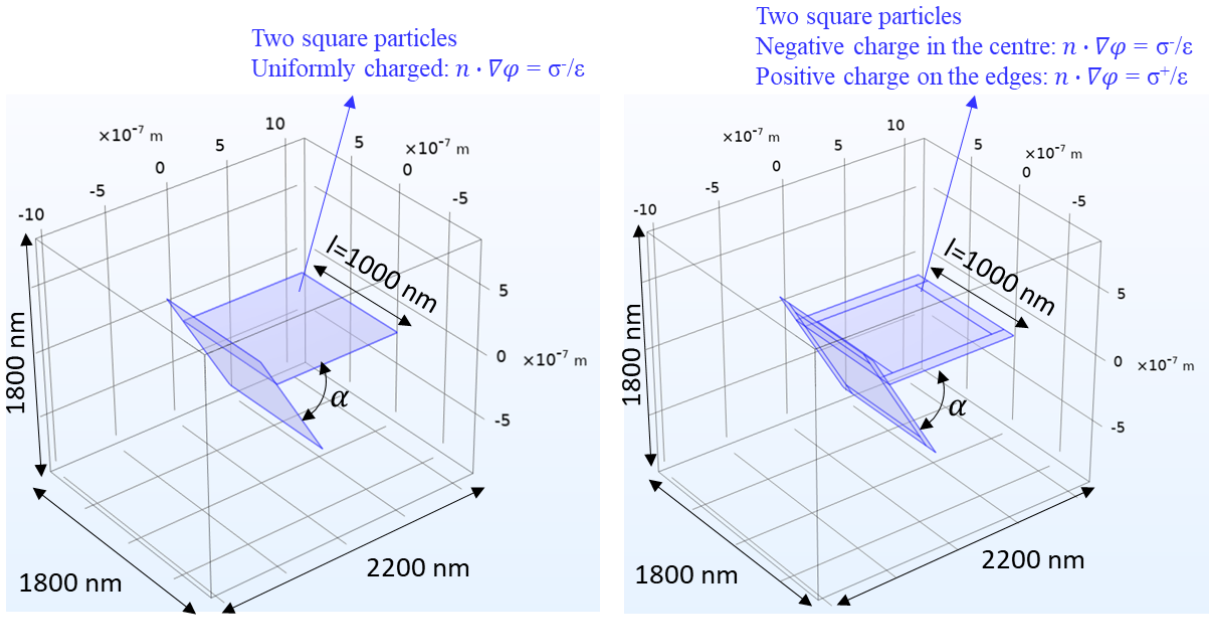

(a) (b)

Figure 6. Finite element models used to solve the Poisson-Boltzmann equation between two interacting particles in edge-to-face configuration: (a) with uniform negative charge; (b) with positively charged edges and negatively charged surface.

5 RESULTS AND DISCUSSION

The results are presented hereafter for the face-to-face and edge-to-face configurations, respectively. The discussion focuses on the capability of each interaction mechanism to explain the thermo-mechanical behaviour of clays observed at the macroscale. This includes the behaviour under mechanical compression at different temperatures (stress-thermal paths 1 and 2 in Figure 7) and the volumetric response during heating and subsequent cooling for OC clays (stress-thermal path 3 in Figure 7) and NC clays (stress-thermal path 4 in Figure 7). Differences between uniformly negatively charged particles and particles with positively charged edges are investigated and discussed. The first case is considered representative of clays saturated with water solution at high pH (Figure 2b), while the second is considered representative of clays saturated with water solution at low pH (Figure 2a).

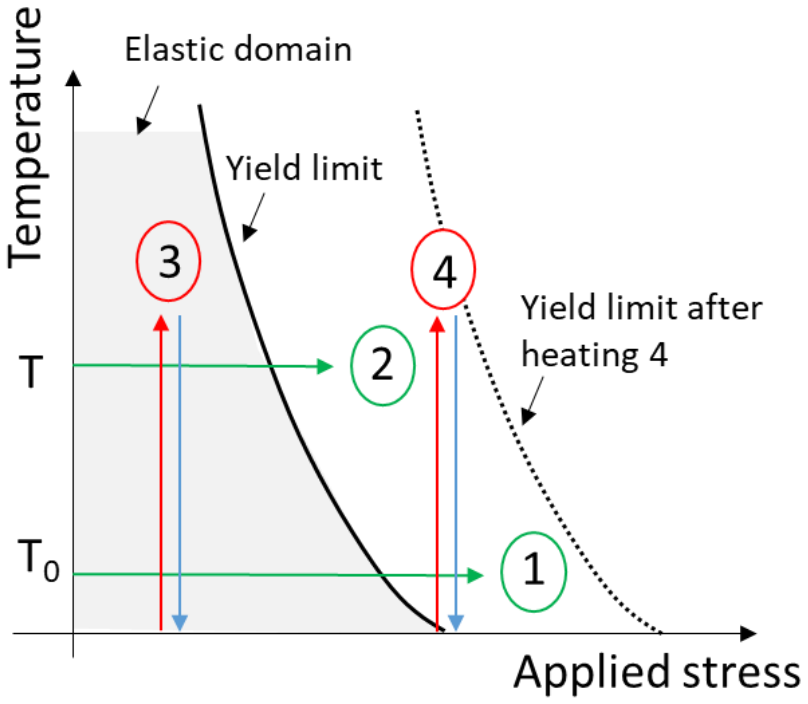

Figure 7. Methodology and analysis of the stress-temperature paths. Green paths indicate loading at constant temperature (paths 1 and 2). Red and blue paths indicate heating and cooling at constant stress, respectively (paths 3 and 4).

5.1 Face-to-face configuration

The electrostatic potential field obtained for the face-to-face configuration is plotted in Figure 8a for the case of uniformly negatively charged particles and Figure 8b for the case of particles with positively charged edges, along a line parallel to one particle plane and passing through its barycentre (black line on the left figures), at different temperatures. As expected, the potential is higher in the case of uniformly charged particles (Figure 8a) as the total charge is higher, and it increases with increasing temperature. In the case of uniformly charged particles, the electrostatic potential decays only outside the particle; in the case of positively charged edges, the electrostatic potential starts decaying inside the particle and is almost nil outside the particle footprint (this is the reason why a smaller volume domain could be considered for the case of positively charged edges).

The electrostatic potential field is plotted in Figure 9a in the case of particles with positively charged edges and in Figure 9b in the case of uniformly negatively charged particles, on a line perpendicular to the particles planes (black line on the upper figures) for a separation distance between the particles of 100 nm. The electrostatic potential at particle mid-distance increases with temperature indicating higher repulsive force as temperature increases. This effect is more pronounced for the particles with positively charged edges. The decay of electrostatic potential outside the particles is similar for the two cases.

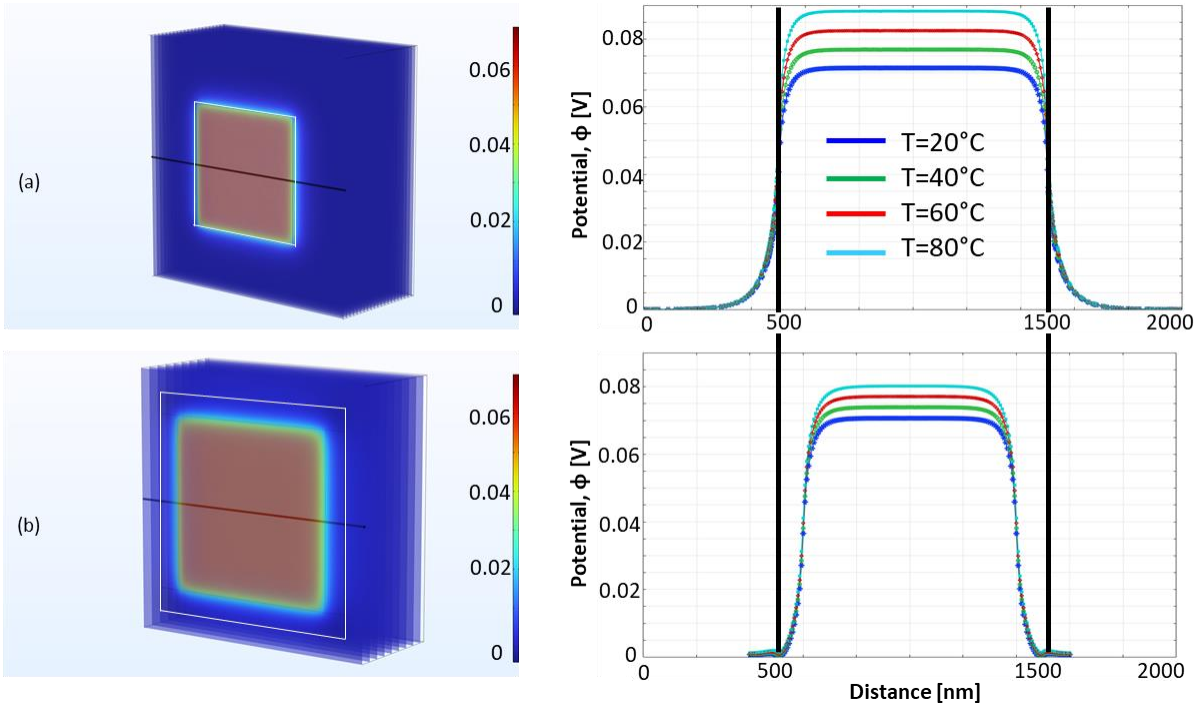

Figure 8. Electrical potential field at 20 °C around a particle interacting with another particle in face-to-face configuration and its distribution along the particle axis for different temperatures: (a) uniformly negatively charged particle and (b) particle with positively charged edges.

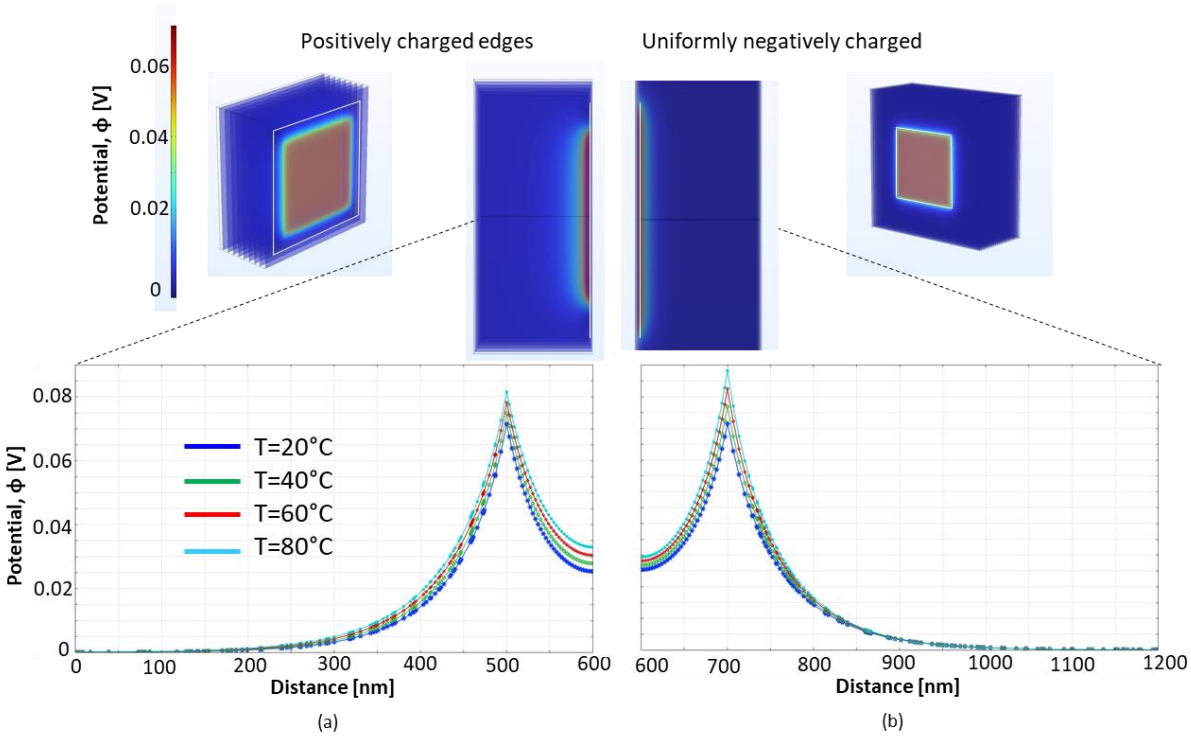

Figure 9. Electrical potential field at 20°C in the perpendicular direction to a particle surface interacting with another particle in face-to-face configuration, and its distribution for different temperatures for (a) particles with positively charged edges and (b) uniformly negatively charged particles.

The electrochemical force per unit particle surface area, including the Coulombic and the van der Waals interactions, as a function of the separation distance between two face-to-face particles is plotted in Figure 10a for the uniformly negatively charged particles and in Figure 10b for the particles with positively charged edges. The curves are presented for different temperatures. Positive force is repulsive, while negative force is attractive. At a short inter-particle distance, the attractive van der Waals force prevails (ascending branch). In contrast, the attractive interaction disappears at distances sufficiently large, and the Coulombic repulsion due to the interacting double layers takes over. At very low separation distance, the interaction between the particles is assumed to be governed by the Born repulsion (black branch on the left), which is considered temperature independent (Israelachvili 2019).

Two mechanical compression paths at 20°C and 80°C are represented by the green arrows (associated with the stress-thermal paths 1 and 2 in Figure 7, respectively). When a mechanical load is applied to two particles at high separation distance, they get closer (the separation distance decreases), and the interaction repulsive force between them increases. Any unloading before reaching the peak of the curve will lead to a recovery of the separation distance,

explaining the elastic behaviour observed at the macroscale for loading at pressures lower than the preconsolidation pressure. The curve peak represents a force barrier; once the barrier is overcome, the two particles come into contact on the Born repulsion branch. This is a potential plastic mechanism since this process is associated with a non-recoverable compression (see figure). In this sense, the force barrier can be associated with the macroscopic pre-consolidation (yielding) pressure.

Considering the compression path at higher temperature (stress-thermal path 2 in Figure 7), the force barrier appears to move upwards (Figure 10). The higher the temperature, the higher the yielding stress if plastic deformation were associated with face-to-face aggregation. This is inconsistent with macroscale experimental evidence showing that yielding stress decreases with increasing temperature (Figure 1b).

The evolution of the force-separation curve with temperature does not also explain the plastic volumetric collapse observed experimentally in NC clays upon heating (Figure 1a, stress-thermal path 4 in Figure 7). If plastic deformation were associated with face-to-face aggregation, the force barrier should move downward and not upward with increasing temperature. Only in this case, a state on the right-hand side of the force separation curve would become 'unstable' at higher temperature, and irreversible face-to-face aggregation would be triggered with the two particles coming into contact on the Born repulsion branch.

These two observations lead to excluding face-to-face aggregation as a mechanism underlying plastic thermo-mechanical behaviour. For this reason, frictional dissipation occurring in edge-to-face configuration was investigated as the potential mechanism responsible for thermal plastic deformation (see next section). This aligns with the conclusions drawn for mechanical loading only by Pedrotti and Tarantino (2018), i.e., plastic deformation is mainly associated with frictional sliding at edge-to-face inter-particle contact.

If the force barrier is not exceeded and particles are in non-contact face-to-face configuration (right-hand side of the curve), a heating-cooling cycle at constant applied force is represented by the red and blue arrows. During heating, the separation distance between the particles increases (from black to red curves going from 20 to 80°C), and it is recovered during cooling. The micro-pore between the two facing particles expands when temperature increases and contracts reversible upon cooling. This is consistent with microscopic observation and can explain the thermo-elastic behaviour observed experimentally for OC clays (stress-thermal path 3 in Figure 7).

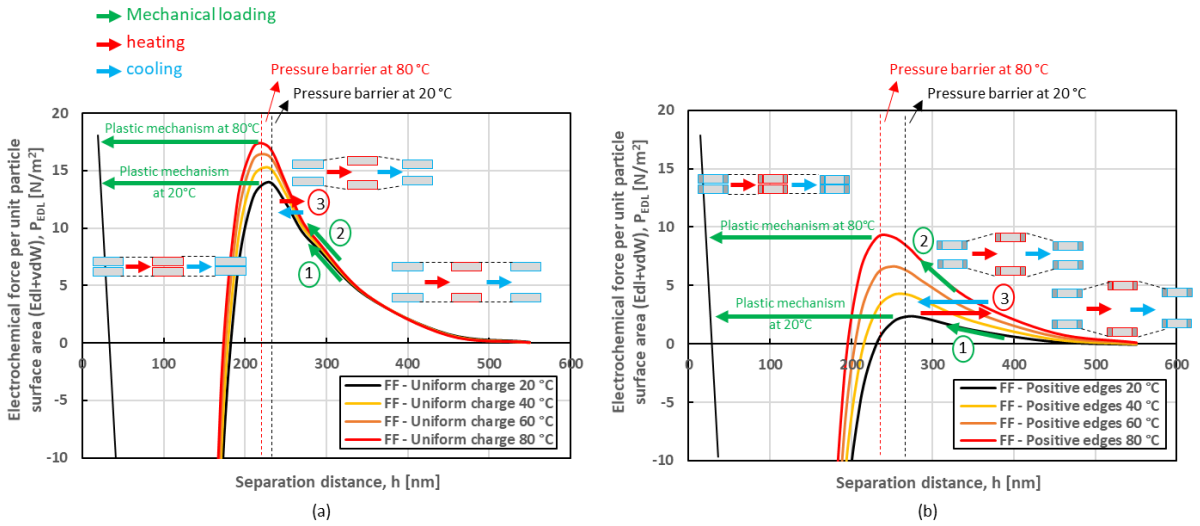

Figure 10. Interaction force (Coulombic plus van der Waals interaction) between two particles in face-to-face configuration: (a) uniform negatively charged particles (high pH); (b) positively charged edges and negatively charged central surface (low pH).

Similar observations can be made for the particles with positively charged edges (Figure 10b). In this case, the repulsive interaction is globally lower because the total negative charge is lower due to the positive edges. In this case, the reversible expansion during thermal loading is more pronounced.

5.2 Edge-to-face configuration

The electrostatic potential field obtained for the edge-to-face configuration at 20°C and for an angle between the particles of 40° is presented in Figure 11a for the case of uniformly negatively charged particles and in Figure 11b for the case of particles with positively charged edges. The difference due to the presence of the positive charge on the edges is clearly visible. Figure 12 gives the evolution of the electrostatic normal force, N_{EDL}, and momentum M_{EDL}, per unit particle surface area due to the double layers interactions of two particles in edge-to-face configuration as a function of the angle between them, for 20 and 80°C, for uniformly negatively charged particles and for particles with positively charged edges. Interestingly, it was found that the electrostatic force was perpendicular to the particle for all configurations ($T_{EDL}\approx 0$ and $N_{EDL}\approx P_{EDL}$, Figure 4).

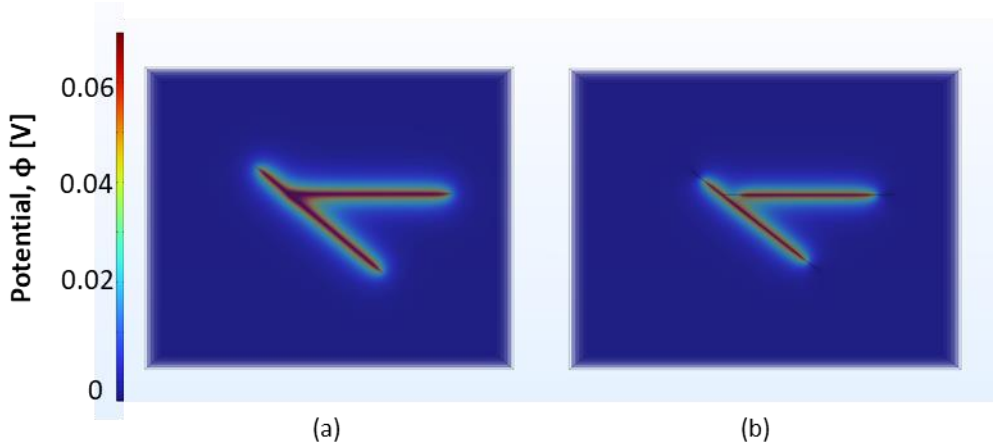

Figure 11. Potential field at 20°C in a system of two edge-to-face particles with an angle of 40° between them, in the case of (a) uniformly negatively charged particles and (b) particles with positively charged edges.

Both the electrostatic normal force and the moment decrease with the increasing angle between the particles. The more open the structure, the lower the repulsive force, as expected from an intuitive standpoint. The normal force and the moment increase with increasing temperature, meaning that at high temperature, the interaction between the particles tends to generate a more open structure (the distance between the particles barycentre and the angle formed by the two particles both increase). This effect is more pronounced for uniformly charged particles; for the case of positively charged edges, the attraction between the positive edge of one particle and the negative surface charge of the other partially reduces the overall repulsion force.

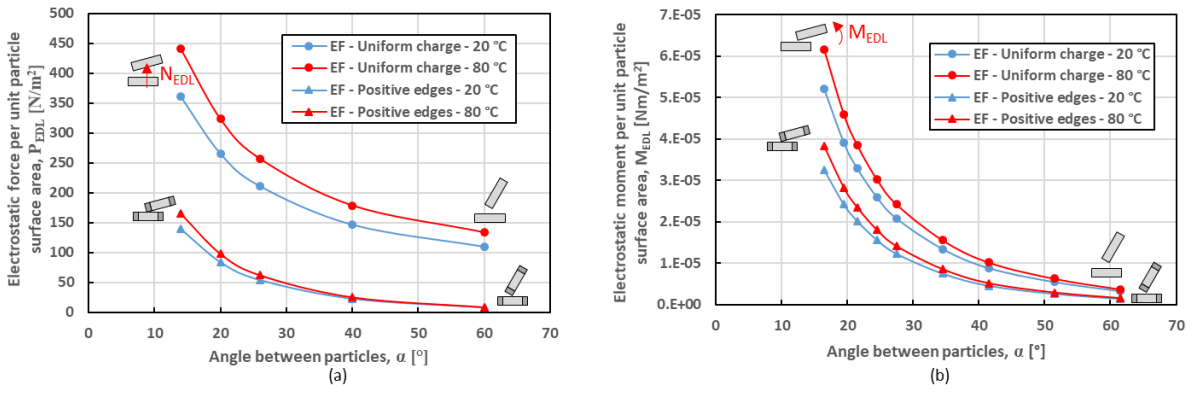

Figure 12. Electric double layers interaction in a system of two particles in edge-to-face configuration, uniformly negatively charged or with positive charges edges, for different angles between the particles: (a) interaction pressure per unit particle surface and (b) bending moment.

The normal component of the contact force per unit particle surface area is plotted in Figure 13a as a function of the applied external force per unit particle surface area for all the considered configurations. In the case of uniformly charged particles, the contact normal force becomes

negative for low external load (large angles between the particles, 60°), indicating that the contact is lost in those cases owing to the repulsion that prevails. This is not the case for the particles with positively charged edges, in which the contact is preserved for all the considered configurations because of the attraction between the positive edge of one particle and the negative surface of the other.

At a given applied external force, the increase in temperature results in a decrease of the normal contact force, potentially favouring the sliding between particles. This effect is less pronounced in the case of particles with positively charged edges due to the edge-to-face attraction. The mobilised friction angle at the contact between the two particles can be determined from Eq. [12]. The mobilised friction angle as a function of the applied external force is presented in Figure 13b.

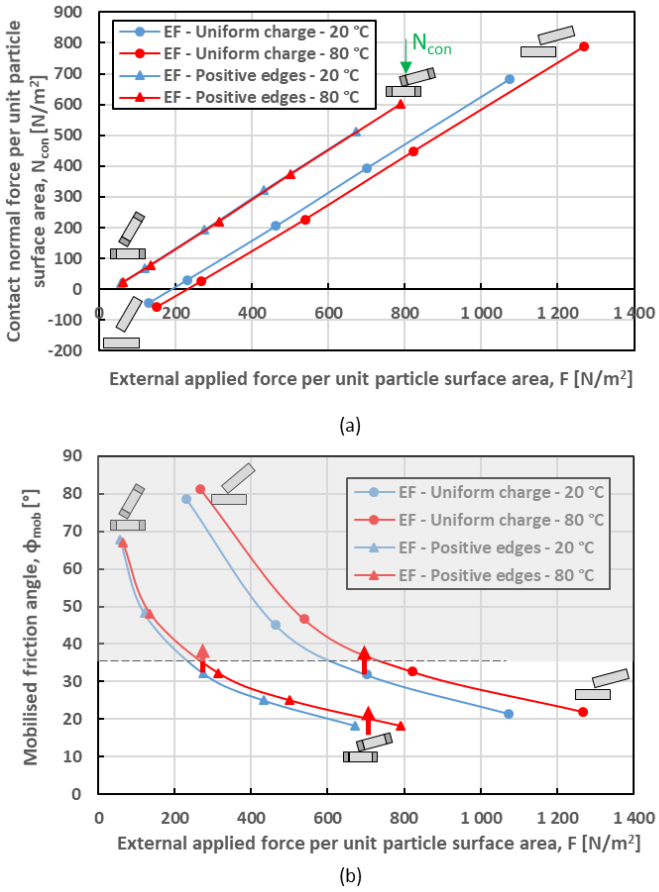

Figure 13. Effect of temperature (a) on the contact pressure per unit particle surface and (b) on the mobilised friction angle at the contact point between two particles in edge-to-face configuration, uniformly negatively charged or with positively charged edges.

The effect of temperature is more evident in this plot; for both uniformly charged particles and particles with positively charged edges, the increase in temperature induces an increase in the

mobilised friction angle. Assuming, as an example, a friction angle equal to 35°, it can be observed that the temperature increase results in a mobilised friction angle overcoming the friction angle for some configurations, in turn triggering the sliding between the particles and consequent plastic volume reduction. This is a possible microscopic mechanism explaining the thermal volumetric plastic collapse observed macroscopically in NC clays (stress-thermal path 4 in Figure 7). The results also show that the effect of temperature depends on the applied external load being more relevant for higher loads, i.e. for less open structures. The dependency of the thermal plastic deformation of NC clays on the applied external load is still an open question in the literature (Sultan et al. 2002, Favero et al. 2016, Houhou et al. 2021) and is being investigated by the authors in a parallel study (Casarella et al. 2024a).

It is also worth noticing that particles with positively charged edges (mimicking kaolinite particles in acidic environment) are stable at lower pressures as opposed to uniformly negatively charged particles (mimicking kaolinite particles in alkaline environment). This may explain the more open structure observed at low to medium stresses in kaolinite prepared with an acidic solution (flocculated structure) compared to the denser fabric kaolinite prepared with an alkaline solution (dispersed structure), as observed by Pedrotti and Tarantino (2018).

6 CONCLUSIONS

The work presented in this paper proposes a microscopic interpretation of the thermo-mechanical volumetric behaviour of non-active clays observed at the macroscale. The non-contact (including Coulombic forces resulting from the double layers interaction and van der Waals forces) and contact forces acting between clay particles, and the effect of temperature on these forces, are discussed and modelled following a combined numerical and analytical approach. Two particle interactions, in face-to-face and edge-to-face configurations, have been analysed, considering both uniformly negatively charged particles (representative of clay in alkaline environment with pH>5-6) and particles with positively charged edges (representative of clay in an acidic environment with pH<5). According to the simplified proposed approach (interaction between only two squared particles with infinitesimal thickness), the main conclusions can be summarised as follows:

- Face-to-face non-contact forces (Coulombic + van der Waals) cannot explain the behaviour of clay under mechanical compression at higher temperatures (stress path 2

in Figure 7), as the decrease of the preconsolidation pressure with temperature is not reproduced;

- Face-to-face non-contact forces (Coulombic + van der Waals) evolution with temperature can explain the thermo-elastic volumetric response observed macroscopically in OC clays (stress path 3 in Figure 7), i.e., clay dilates during heating, and this deformation is recovered during cooling. The analysis of face-to-face interaction shows indeed that particle separation distance increases with increasing temperature, and this is recovered during subsequent cooling;
- Face-to-face non-contact forces (Coulombic + van der Waals) evolution with temperature cannot explain the thermo-plastic deformation observed macroscopically in NC clays upon heating (stress path 4 in Figure 7);
- Edge-to-face non-contact forces (Coulombic + van der Waals) evolution with temperature (Figure 12) reveals an additional mechanism explaining the thermo-elastic volumetric response observed macroscopically for OC clays (the particles form a more open configuration with increasing temperature, i.e., the clay dilates, and this deformation is recovered during cooling);
- Edge-to-face contact forces decrease with increasing temperature because of the increase of the non-contact forces arising from the electrical double layer interactions. The reduction of the contact force results in an increase of the mobilised friction angle at the contact between the two particles, which may lead to sliding and collapse for some critical configurations. This would explain the plastic deformation associated with heating in NC clays (stress-thermal path 4 in Figure 7).

This work was an attempt to investigate the possible physical sources which stand at the orgin of the peculiar behaviour of clays submitted to temperature changes. The study is limited to the interaction between two squared particles with infinitesimal thickness, and it is meant to be a preliminary analysis of the mechanisms involved at the clay particle scale that might affect the response at the macroscale, without claming to find a definitive solution to such complex problem. Currently, improvements are under development, in particular to take into account more representative shape and thickness of the particles, as well as the charge distribution on the particles themselves. As mentioned in the introduction, the analysis is limited to two particles interactions, and a proper upscale approach is needed to extend the results to a larger number of particles. In further work, the obtained results could feed a CGMD type model, by

providing data to define and calibrate a physically-based energy function governing the interaction between particles.

ACKNOWLEDGEMENTS

This work was funded by the ANR project GEO2 (ANR-19-CE05-0003-01). The Laboratory 3SR is part of the LabEx Tec 21 (Investissement d'avenir – grant agreement n. ANR-11-LABX-0030).

LIST OF SYMBOLS

a [m]	horizontal component of the lever arm of the applied external force
d [m]	lever arm of the external force parallel to the particle axis
dx [m]	displacement perturbation in the x-direction
dz [m]	displacement perturbation in the z-direction
e [C]	charge of the electron
h [m]	inter-particle distance
k [J K^{-1}]	Boltzmann constant
l [m]	squared particle side size
n [-]	vector normal to the particle surface
n_0 [ions/m^3]	reference ions concentration
t [m]	clay particle thickness
x	x-coordinate in space
y	y-coordinate in space
z	z-coordinate in space
A [m^2]	particle surface area
A_H [-]	Hamaker constant

F [N]	external applied force
F_n [N]	normal component of the applied external force
F_t [N]	tangential component of the applied external force
M_{EDL} [Nm]	electrostatic interaction moment
N_{con} [N]	normal component of the contact force
N_{EDL} [N]	normal component of the electrostatic interaction force
P_{con} [N]	contact force
P_{EDL} [N]	electrostatic interaction force
T [°C]	temperature
T_0 [°C]	reference temperature
T_{con} [N]	tangential component of the contact force
T_{EDL} [N]	tangential component of the electrostatic interaction force
U_{EDL} [J]	electrostatic free energy
U_{vdW}[J]	van der Waals interaction energy
V [m^3]	system volume
X_{Edl}[N]	Interaction electrostatic force in the x-direction
X_{vdW}[N]	van der Waals interaction force
Y_{Edl} [N]	Interaction electrostatic force in the y-direction

α [°]	angle between the particles
ϵ [$C^2J^{-1}m^{-1}$]	dielectric permittivity
ϵ_0 [$C^2J^{-1}m^{-1}$]	dielectric permittivity in vacuum
ϵ_r [-]	relative dielectric permittivity

ε_v [%] volumetric strain

φ_{mob}[°] mobilised friction angle

ϕ [V] electrical potential

σ [C/m^2] charge density on the particle surface

σ'_p [Pa] pre-consolidation pressure

θ [°] angular coordinate

$d\theta$ [°] angular perturbation

ν [-] valence

$\Omega - \Omega_0$[J] Grand Potential

REFERENCES

Abuel-Naga, H.M., Bergado, D.T., Bouazza, A., and Pender, M. 2009. Thermomechanical model for saturated clays. Géotechnique, **59**(3): 273–278.

Baldi, G., Hueckel, T., and Pellegrini, R. 1988. Thermal volume changes of the mineral-water system in low porosity clay soils. Canadian Geotechnical Journal, **25**(4): 807–825.

Boudali, M., Leroueil, S., and Srinivasa Murthy, B.R. 1994. Viscous behaviour of natural clays.

Brochard, L., Honório, T., Vandamme, M., Bornert, M., Brochard, L., Honório, T., Vandamme, M., Bornert, M., Nanoscale, M.P., and T, L.B. 2017. Nanoscale origin of the thermo-mechanical behavior of clays. Acta Geotechnica, **12**(4): 1261–1279.

Burghignoli, A., Desideri, A., and Miliziano, S. 2000. A laboratory study on the thermomechanical behaviour of clayey soils. Canadian Geotechnical Journal, **37**(4): 764–780. doi:10.1139/cgj-37-4-764.

Campanella, R.G., and Mitchell, J.K. 1968. Influence of temperature variations on soil behavior. Journal of the Soil Mechanics and Foundations Division, ASCE, **94**(3): 709–734.

Carrier, B. 2014. Influence of water on the short-term and long-term mechanical properties of

swelling clays: experiments on self-supporting films and molecular simulations.

Casarella, A. 2022. Multi-scale investigation of the thermomechanical behaviour of non-active clay. PhD thesis, Université Grenoble Alpes.

Casarella, A., Tarantino, A., and Di Donna, A. 2023a. Micromechanical interpretation of the thermoplasticity of normally consolidated clay. Géotechnique, (under prep).

Casarella, A., Tarantino, A., Richefeu, V., and Di Donna, A. 2023b. Evaluation of Gay-Berne interaction potential to simulate 3D DLVO interaction of finite clay particles. Computers and Geotechnics, **under revi**.

Cekerevac, C., and Laloui, L. 2004. Experimental study of thermal effects on the mechanical behaviour of a clay. International Journal for Numerical and Analytical Methods in Geomechanics, **28**(3): 209–228.

Coccia, C.J.R., and McCartney, J.S. 2016. Thermal volume change of poorly draining soils II: Model development and experimental validation. Computers and Geotechnics, **80**: 16–25.

Cui, Y.J., Sultan, N., and Delage, P. 2000. A thermo-mechanical model for saturated clays. Canadian Geotechnical Journal, **620**: 607–620.

Derjaguin, B., and Landau, L. 1941. Theory of the stability of strongly charged lyophobic soils and of the adhesion of strongly charged particles in solutions of electrolytes. Acta Physicochimica URSS, **14**(6): 633–662.

Di Donna, A., Barla, M., and Amis, T. 2017. Energy Geostructures : Analysis from research and systems installed around the World. *In* DFI 42th Annual Conference on Deep Foundations, New Orleans, USA.

Di Donna, A., and Laloui, L. 2015. Response of soil subjected to thermal cyclic loading: Experimental and constitutive study. Engineering Geology, **190**: 65–76.

Ebrahimi, D., Pellenq, R.J.M., and Whittle, A.J. 2016. Mesoscale simulation of clay aggregate formation and mechanical properties. Granular matter, **18**: 1–8.

Eriksson, L.G. 1989. Temperature effects on consolidation properties of sulphide clays. *In* Proceedings of the 12th international conference on soil mechanics and foundation

engineering. Rio de Janeiro. pp. 2087–2090.

Favero, V., Ferrari, A., and Laloui, L. 2016. Thermo-mechanical volume change behaviour of Opalinus Clay. International Journal of Rock Mechanics and Mining Sciences, **90**: 15–25.

Frost, R., Kloprogge, T., and Kristóf, J. 2004. Raman and infrared spectroscopic study of modification of kaolinite surfaces by intercalation. Interface Science and Technology,: 184–215.

Graham, J., Tanaka, N., Crilly, T., and Alfaro, M. 2001. Modified Cam-Clay modelling of temperature effects in clays. Canadian Geotechnical Journal, **38**(3): 608–621.

Gupta, A., Govind Rajan, A., Carter, E.A., and Stone, H.A. 2020. Thermodynamics of electrical double layers with electrostatic correlations. Journal of Physical Chemistry, **124**(49): 26830–26842.

Gupta, V., and Miller, J.D. 2010. Surface force measurements at the basal planes of ordered kaolinite particles. Journal of Colloid and Interface Science, **344**(2): 362–371.

Güven, N. 1992. Rheological aspects of aqueous smectite suspensions, in Clay-Water Interface and Its Rheological Implications. *In* CMS Workshop Lect. *Edited by* and R.M.P. N. Güven. pp. 81–127.

Houhou, R., Sutman, M., Sadek, S., and Laloui, L. 2021. Microstructure observations in compacted clays subjected to thermal loading. Engineering Geology, **287**: 105928.

Hueckel, T., and Baldi, G. 1990. Thermoplasticity of saturated clays: experimental and constitutive study. Journal of Geotechnical Engineering, **116**(12): 1778–1796.

Israelachvili, J.N. 2019. Intermolecular and Surface Forces.

Laloui, L., and Di Donna, A. 2013. Energy geostructures: innovation in underground engineering. ISTE Ltd and John Wiley & sons Inc.

Malmberg, C.G., and Maryott, A.A. 1956. Dielectric constant of water from 0 to 100 C. Journal of Research of the National Bureau of Standards, **56**(1): 1.

Masliyah, J.H., and Bhattacharjee, S. 2006. Electric Double Layer. In Electrokinetic and Colloid Transport Phenomena.

Mitchell, J.K., and Soga, K. 2005. Fundamentals of soil behavior. John Wiley.

Modaressi, H., and Laloui, L. 1997. A thermo-viscoplastic constitutive model for clays. Internation journal for numerical and analytical method in geomecanics, **21**(5): 313–335.

Moritz, L. 1995. Geotechnical properties of clay at elevated temperatures. Swedish Geotechnical Institute report, **47**.

Del Olmo, C., Fioravante, V., Gera, F., Hueckel, T., Mayor, J.C., and Pellegrini, R. 1996. Thermomechanical properties of deep argillaceous formations. Engineering Geology, **33**: 87–101.

Parsegian, V.A., and Ninham, B.W. 1970. Temperature-Dependent van der Waals Forces. Biophysical Journal, **10**(7): 664–674. Elsevier.

Pedrotti, M., and Tarantino, A. 2017. An experimental investigation into the micromechanics of non-active clays. Géotechnique, **68**(8): 666–683.

Pedrotti, M., and Tarantino, A. 2018. A conceptual constitutive model unifying slurried (saturated), compacted (unsaturated) and dry states. Géotechnique,: 1–79.

Romero, E., Villar, M. V., and Lloret, A. 2005. Thermo-hydro-mechanical behaviour of two heavily overconsolidated clays. Engineering Geology, **81**(3): 255–268.

Sridharan, A., and Rao, G. 1973. Mechanism controlling volume change of saturated clays and the role of the effective stress concept. Géotechnique, **23**: 359–382.

Sulem, J., Lazar, P., and Vardoulakis, I. 2007. Thermo-poro-mechanical properties of clayey gouge and application to rapid fault shearing. International Journal for Numerical and Analytical Methods in Geomechanics, **31**(3): 523–540.

Sultan, N., Delage, P., and Cui, J.Y. 2002. Temperature effects on the volume change behaviour of Boom clay. Engineering Geology, **64**: 135–145.

Tidfors, M., and Sällfors, G. 1989. Temperature effects on preconsolidation pressure. Geotechnical Testing Journal, **12**(1): 93–97.

Towhata, I., Kuntiwattanaku, P., Seko, I., and Ohishi, K. 1993. Volume change of clays induced by heating as observed in consolidation tests. Soils and Foundations, **33**(4): 170–183.

Verwey, E.J.W., and Overbeek, J. 1948. Three-dimensional discrete element method of analysis of clays. *In* Elsevier, Amsterdam.